การประดิษฐ์เซลล์สุริยะฟิล์มบาง CIGS โดยซีลีไนเซชันของชั้นโลหะ

นางสาวขวัญฤทัย บุตรศรีรักษ์

วิทยานิพนธ์นี้เป็นส่วนหนึ่งของการศึกษาตามหลักสูตรปริญญาวิทยาศาสตรมหาบัณฑิต
สาขาวิชาฟิสิกส์ ภาควิชาฟิสิกส์
คณะวิทยาศาสตร์ จุฬาลงกรณ์มหาวิทยาลัย
ปีการศึกษา 2557

FABRICATION OF CIGS THIN FILM SOLAR CELLS BY SELENIZATION OF METALLIC LAYERS

Miss Kwanruthai Butsriruk

A Thesis Submitted in Partial Fulfillment of the Requirements
for the Degree of Master of Science Program in Physics
Department of Physics
Faculty of Science
Chulalongkorn University
Academic Year 2014

Thesis Title	FABRICATION OF CIGS THIN FILM SOLAR CELLS BY SELENIZATION OF METALLIC LAYERS
By	Miss Kwanruthai Butsriruk
Field of Study	Physics
Thesis Advisor	Assistant Professor Sojiphong Chatraphorn, Ph.D.

Accepted by the Faculty of Science, Chulalongkorn University in Partial Fulfillment of the Requirements for the Master's Degree

.....Dean of the Faculty of Science
(Professor Supot Hannongbua, Dr.rer.nat.)

THESIS COMMITTEE

.....Chairman
(Assistant Professor Rattachat Mongkolnavin, Ph.D.)
.....Thesis Advisor
(Assistant Professor Sojiphong Chatraphorn, Ph.D.)
.....Examiner
(Assistant Professor Nuttakorn Thubthong, Ph.D.)
.....External Examiner
(Rachsak Sakdanuphab, Ph.D.)

ขวัญฤทัย บุตรศรีรักษ์ : การประดิษฐ์เซลล์สุริยะฟิล์มบาง CIGS โดยซีลีไนเซชันของชั้นโลหะ (FABRICATION OF CIGS THIN FILM SOLAR CELLS BY SELENIZATION OF METALLIC LAYERS) อ.ที่ปรึกษาวิทยานิพนธ์หลัก: ผศ. ดร. โศจิพงศ์ ฉัตราภรณ์, 48 หน้า.

ฟิล์มบางสารตั้งต้นโลหะ คอปเปอร์อินเดียมแกลเลียม (CIG) ถูกประดิษฐ์บนแผ่นรองรับกระจกโซดาลาม์ที่เคลือบด้วยโมลิบดีนัม (Mo/SLG) เพื่อเลียนแบบการปลูกสารตั้งต้นโดยวิธีสปัตเตอริงร่วมกัน (Co-sputtering) จากเป้าโลหะ ซีลีเนียม (Se) ถูกนำมารวมเข้าเป็นหนึ่งเดียวกัน โดยการระเหยของ คอปเปอร์-ซีลีเนียม (Cu-Se) และ ไอ Se แต่คอปเปอร์ (Cu), อินเดียม (In) และ แกลเลียม (Ga) ไม่สามารถปลูกพร้อมกัน เนื่องจากจุดหลอมเหลวของ In ค่อนข้างต่ำ จึงทำให้เกิดการรวมตัวกันเป็นกลุ่มก้อนของสารตั้งต้น ดังนั้นการเรียงลำดับการปลูกโดยการระเหยของธาตุ คอปเปอร์-แกลเลียม (Cu-Ga) แล้วตามด้วย In จะถูกนำมาใช้ เมื่ออุณหภูมิของแผ่นรองรับต้องเหมาะสมต่อการสะสมของชั้น Cu-Ga และ In ซึ่งมีผลต่อรูปแบบของธาตุโลหะผสมของสารตั้งต้น จึงมีขั้นตอนการแอนนีล (anneal) ในระบบสุญญากาศ ที่อุณหภูมิ 450 องศาเซลเซียส โดยที่ระยะเวลาของการระเหย Cu-Se และการให้ความร้อนแก่แผ่นรองรับ จะเป็นตัวดำเนินการสำคัญที่มีการเปลี่ยนแปลง รูปแบบของชั้น CIGS และเฟสซาลโคไพไรท์จะถูกวิเคราะห์โดย กล้องจุลทรรศน์อิเล็กตรอนแบบส่องกราดที่มีกำลังขยายสูง (FESEM) และเครื่องวิเคราะห์การเลี้ยวเบนรังสีเอ็กซ์ (XRD) ตามลำดับ เมื่อเซลล์แสงอาทิตย์ชนิดฟิล์มบาง CIGS ถูกสร้างขึ้นโดยขั้นตอนมาตรฐาน และจะถูกทดสอบด้วยเครื่องวิเคราะห์คุณลักษณะกระแส-แรงดันไฟฟ้า (I-V measurement) ของเซลล์แสงอาทิตย์ และการตอบสนองเชิงสเปกตรัมของแสงจะใช้เครื่องวัดประสิทธิภาพควอนตัม (QE measurement) ซึ่งประสิทธิภาพที่ดีที่สุดสำหรับเซลล์แสงอาทิตย์ CIGS ที่ได้รับโดยการประดิษฐ์ชั้นดูดกลืนแสงด้วยวิธีนี้คือ 13.2 เปอร์เซ็นต์

ภาควิชา ฟิสิกส์ ลายมือชื่อนิสิต .....

สาขาวิชา ฟิสิกส์ ลายมือชื่อ อ.ที่ปรึกษาหลัก .....

ปีการศึกษา 2557

5571928023 : MAJOR PHYSICS
KEYWORDS: CIGS, THIN FILM SOLAR CELLS, CO-EVAPORATION, SELENIZATION.

KWANRUTHAI BUTSRIRUK: FABRICATION OF CIGS THIN FILM SOLAR CELLS BY SELENIZATION OF METALLIC LAYERS. ADVISOR: ASST. PROF. SOJIPHONG CHATRAPHORN, Ph.D., 48 pp.

Cu-In-Ga (CIG) metallic precursor thin films were fabricated on Mo-coated soda-lime glass (SLG) substrates to imitate the precursor growth by co-sputtering from metallic targets. Selenium (Se) was incorporated into the precursors by means of Cu-Se co-evaporation and Se vapor. It was found that Cu, In and Ga could not be deposited simultaneously due to lower melting point of In that caused the agglomeration of the precursors. The sequential evaporations of Cu-Ga followed by In were then applied. The substrate temperature was optimized for the depositions of Cu-Ga and In that directly affected the formation of the alloying precursors. The vacuum annealing of precursors at 450°C was employed. The duration of the Cu-Se flux and the annealing time were among the important varying parameters. The formation of the CIGS layer and its chalcopyrite phases were investigated by FESEM and XRD, respectively. The CIGS thin film solar cells were also fabricated by standard procedures and tested for their I-V characteristics and spectral response by quantum efficiency measurements. The best efficiency of the CIGS solar cells obtained from the absorber fabricated by this method is 13.2%.

Department:	Physics	Student's Signature	.....
Field of Study:	Physics	Advisor's Signature	.....
Academic Year:	2014		

ACKNOWLEDGEMENTS

It is a genuine pleasure to express my deep sense of thanks and gratitude to my mentor - thesis advisor, Assistant Professor Dr. Sojiphong Chatraphorn. His dedication and keen interest above all his overwhelming attitude to help his students had been solely and mainly attributable for completing my work. His timely advice, scientific skill, scholarly advice and valuable suggestions have helped me to a very great extent to accomplish this thesis.

I would like to give thanks for suggestion from my thesis committee: Assistant Professor Dr. Rattachat Mongkolnavin, Assistant Professor Dr. Nuttakorn Thubthong and Dr. Rachsak Sakdanuphab.

I thank all the members of Semiconductor Physics Research Laboratory (SPRL); Miss Boonyaluk Namnuam, Miss Busarin Noikaew and master degree students for their kind help, encouragement, technical suggestions and co-operation throughout my study period.

I would like to acknowledge the financial supports from Thailand Center of Excellence in Physics (ThEP Center), the Ratchadaphisek Somphot Endowment Fund (2013), Chulalongkorn University (Sci-Super CU-56-013-FC), and the Special Task Force for Activating Research (STAR), Chulalongkorn University through the Energy Materials Physics Research Group Research Group.

I would like to thank the Department of Geology, Faculty of Science, Chulalongkorn University for allowing me to access the x-ray diffraction (XRD) facility.

I am extremely thankful to my friends for providing me necessary E-THESIS program suggestions during my research pursuit.

Finally, I owe a deep sense of gratitude to my parents who always give me their constant encouragement throughout my study.

CONTENTS

Page

LIST OF TABLES

Page

LIST OF FIGURES

Page

Page

CHAPTER I
INTRODUCTION

1.1 Overview

A greenhouse effect has been known to increase carbon dioxide gas in the Earth's atmosphere and reduce prevention of solar radiation resulting in a global climate change. This is partly due to the combustion of fossil fuel. The consumption of the fossil fuel will forcibly come to an end. Thus, alternative sources of energy are needed to replace or slow down the use of fossil fuel. A Solar cell or photovoltaic device is one of considerable sources of energy. A first solar cells by Becquerel was made in 1839 with a cuprous oxide thin film solar cell [1]. Then, in 1870s, Willoughby Smith, W. G. Adams, and R. E. Day discovered a photovoltaic (PV) effect in selenium. Three years later, a sheet of amorphous selenium on a metal backing and covered the selenium with a transparent gold leaf film was replaced by C. E. Fritts. About 75 years later when quantum mechanics became well known, a p-n was invented. In 1954, at Bell Laboratory a silicon single crystal solar cell was created with efficiency up to 6% [2]. In 1958, n-on-p silicon PV cells are fabricated by U.S. Signal Corps Laboratories that achieves 9% efficiency. A cadmium sulfide (CdS) PV system was established by French scientists and the Institute of Energy Conversion at the University of Delaware for research and development on thin-film photovoltaic (PV) and solar thermal systems and became the world's first laboratory dedicated to PV research and development in 1973 [2]. After 1973, solar cells are an excellent power source for the people of Africa. This gave governments and scientists even more reason to try to find ways to improve solar power technology. In the 1980s, an engineer named Bill Yerks invented a new kind of PV cell that were made by screen printing a mix of silver glue with glass. In the 1990s, PV cells were built into flexible plastic sheets [3]. Today, silicon-based solar cell is the most common type of solar cells, which is quite expensive for those with high efficiencies. To decrease cost for the fabrication of the silicon-base on solar cells, new kinds of solar cells were developed such as polycrystalline silicon, III-V group single crystal with multi-junction, thin films and dye-sensitized solar cells, etc. Solar cell efficiency records as an evolution of the different solar cell performances is shown in Fig. 1. Thin film

devices' performance is the most attractive, particularly copper indium gallium diselenide ($CuIn_{1-x}Ga_xSe_2$) or CIGS. As of 2015, ZSW, Germany has confirmed the efficiency of CIGS around 21.7 % [4].

1.2 Fabrication methods of $Cu(In,Ga)Se_2$ thin films

The CIGS thin film is a ternary compound semiconductor of I-III-VI_2 group whose energy gap is between 1.02 – 1.68 eV. The bandgap energy (E_g) can be adjusted by varying the ratio of In and Ga atoms. The x value is the ratio of Ga to group-III elements, i.e. x = [Ga]/([In]+[Ga]), in the fabrication of the CIGS thin films and can be varied from 0 to 1. The y value is the ratio of Cu to group-III elements, i.e. y = [Cu]/([In]+[Ga])). Due to high absorbtion coefficient of CIGS, it has been used as photon absorber layer in high efficiency thin film solar cell. The structure of CIGS thin film solar cells is a multi-layer material, e.g. Al-grid/ZnO/CdS/CIGS/Mo/SLG. Mo is a back electrical contact coated on soda lime glass (SLG) substrate while Al-grid is a front electrical contact. The CIGS layer and the ZnO layer are p-type semiconductor and n-type semiconductor, respectively [5]. CIGS thin films can be fabricated by various techniques as summarized in Table 1. For mass production and high throughput process, co-sputtering of metallic targets together with selenization process has been proposed. However, the sputtering process has a difficulty of adjusting the composition in the thin films because it is solely depending on the pre-made sputtering targets. Thus, in this work, I will try to imitate the co-sputtering process by using co-evaporation of metallic precursors and selenization to study physical properties of the CIGS absorbers and investigate the device performances.

Table 1 Fabrication methods for CIGS thin film.

Methods	Advantage	Disadvantage
Co-evaporation [6]**;** evaporate Cu, In, Ga and Se atoms simultaneously	- suitable for studying physical properties - good uniformity	- limit only to lab scale - difficult for large area
Co-sputtering [7]**;** fabricate by simultaneous sputtering of two targets (In target and Cu-Ga alloy target)	- high deposition speed - large area films	- difficult control of composition - expensive targets
Spray solution [8]**;** aqueous solution containing $CuCl_2$, $InCl_3$, $Ga(NO_3)_3H_2O$ and selenourea was used for precursor solution and vaporized as aerosol before deposition at T_{sub} = 400ºC	- low-cost - use in large-scale production - does not require the use of vacuum	- difficult to control parameters, e.g. solution flow rate, direction growth and non-uniformity
Selenization [9]**;** Se over-vapor after metallic deposition process (T_{sub} = 550 – 650ºC in vacuum system)	- rapid process	- easy agglomerate of In-Se compound

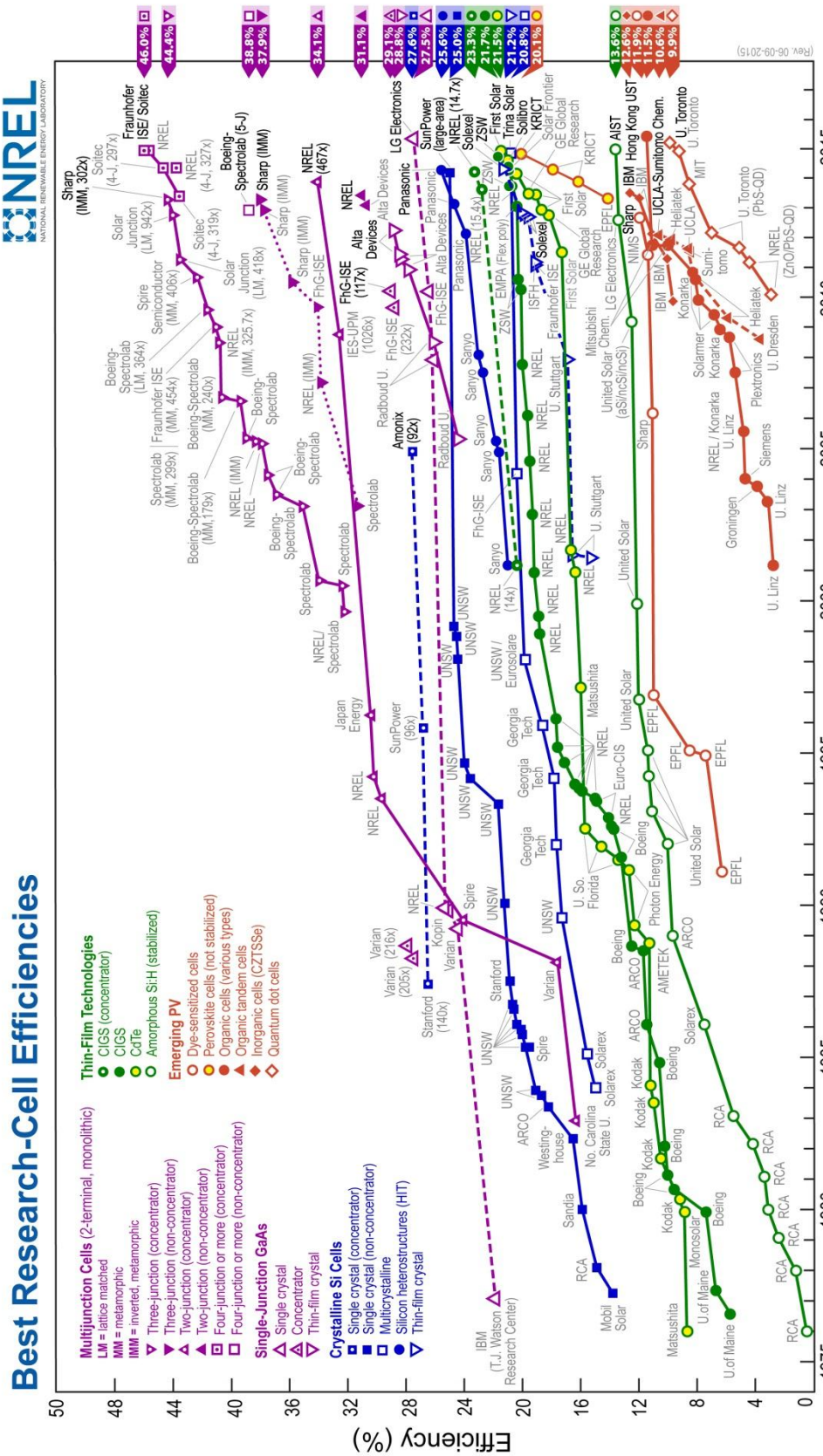

Figure 1 Records of efficiency of various kinds of solar cells [10].

1.3 Selenization techniques

In general, CIGS multisource co-evaporation technique can achieve the CIGS solar cells up to 21.7% [4]. However, this technique is more expensive in terms of metallic material consumption and may not be appropriate for the production of large scale area at present. Thus, the precursors sputtering technique and selenization are studied and some examples are briefly described below.

In 2003, K. Ho and his group at Korea Institute of Energy Research studied the preparation CIGS polycrystalline thin films with the two step method [9]. They prepared CIGS thin films by two step processes. Metallic precursors were deposited on substrate by DC sputtering. When the precursors were finished, it was followed by selenization process using Se vapor. It was found that the crystal structure and morphology of the CIGS thin films depended on the substrate temperature profile and time period during the growth processes. The highest conversion efficiency was 3.48%.

The industrial CIGS solar cell production is based on vacuum systems that it was researched in 2004 by M. Kaelin and his group. The used of simple and non-vacuum systems, which is the choice of the precursor material that has to be made with respect to the selenization conditions to avoid detrimental impurity phases. It achieved efficiencies above 10% [11].

S. Cherng-Yuh and his group studied the CIGS thin films which were prepared by selenization method with two stages in 2011 [7]. At the first stage, soda lime glass substrate coated with CuInGa (CIG) metallic precursors by DC magnetron sputtering with the ratio of Cu:In:Ga of 1:0.7:0.3. The thickness of the CIG precursors is 2-3 μm that the chemical compositions of Cu, In and Ga are 45.9%, 37.9% and 16.1%, respectively. At second stage, the metallic precursors were selenized in a vacuum evaporation system and supplied with Se vapor at 380°C. Annealing was added during the selenization processes by four steps at 100°C, 260°C, 360°C and 550°C, respectively. The chalcopyrite phases of CIGS phase occurred when the selenization temperature was increased to above 360°C. Finally, the annealing at 550°C enhanced quality of the films to achieve the recrystallization and grain growth

process. After the absorber is completed, the 1:1:2 chalcopyrite phase of this work revealed the preferred orientation of (112) plane.

In 2012, researchers from Intermolecular Inc., San Jose, United states, L. Haifan and his group prepared CIGS thin films by two step processes [12]. The Cu-In-Ga precursors and H_2Se gas was used to fabricate the CIGS thin films by evaporation technique. A selenization process was done at high temperature and followed by annealing process to improved crystallinity and properties of the films. The substrate temperature of selenization process was the range of 350-500°C. An intermediate low temperature was added to protect the concentration and binary phase formation that was investigated by X-ray diffraction (XRD) and scanning electron microscopy (SEM). The solar cell with efficiency of 15% was obtained.

The fabrication of CIGS absorber layer with a smooth surface containing a single chalcopyrite phase was obtained in 2013 by J. Han and his group [13]. The precursor was optimized by the deposition of In and Cu-Ga metallic layer for chalcopyrite thin film that Cu-Ga and In layers were fabricated by DC sputtering at room temperature and then annealed at 120°C to enhance diffusion and alloying of Cu-Ga and In layers. The precursors were then selenized by evaporating Se to form CIGS absorber. It was shown that smooth precursor film was the key factor to obtain a homogeneous and compact CIGS film. Unfortunately, this work did not report the efficiency of their solar cells.

In 2013, Tayler B. Harvey and his group studied the CIGS layers from the fabrication process with high temperature selenization process [6]. The CIGS film was obtained by co-evaporation or high temperature annealing of vacuum sputtered metals under selenium vapor. The annealing under inert gas (argon) at 525°C was applied to decrease organic ligands and diffusion of sodium from soda lime glass (SLG) substrate and was also used to solve the rate and property of nanocrystal sintering during selenization at 500°C. Their devices showed the efficiency of 7.1%.

However, in this work, the CIGS absorbers is now proposed by starting with the metallic layers consisting of Cu, In and Ga with appropriate compositions and followed by the selenization of Se vapor which supposedly uses significantly less amount of Se compared to the standard 3-stage co-evaporation technique [14]. When the metallic precursor is finished, it will be supplied with Se by means of Cu-Se co-

evaporation at higher temperature to complete CIGS absorber since Se vapor itself is difficult to diffuse into the precursor. It was found that Cu-Se was believed to be in a liquid phase [15] and was relatively easier to diffuse into the precursor layer and help converting the Cu-Ga-In metallic precursor into CIGS material. The mixing of all constituent elements is expected to be obtained by the diffusion process occurring during the annealing of the films.

1.4 Objectives

A sputtering technique has been proposed to fabricate the CIGS absorbers in a large scale production. But, the sputtering process is relatively difficult to optimize and control the compositions of the elements especially In and Ga. In this work, I will try to mimic the sputtering process by using co-evaporation to form the Cu-In-Ga metallic precursors and find some appropriate methods to incorporate Se into the metallic precursors, and characterize the obtained CIGS absorbers for its crystal structure, compositions, physical appearance as well as the device performances in terms of the current-voltage characteristics and quantum efficiencies.

Expected beneficial outcomes from the thesis are

i) understanding the selenization process for the fabrication of CIGS thin film solar cells,
ii) obtaining the factors affecting the formation of CIGS thin films by selenization process,
iii) obtaining the growth recipe for the CIGS by the selenization process,
iv) obtaining device performance fabricated by this method.

1.5 Outline of thesis

This thesis consists of five chapters. The detailed backgrounds of CIGS materials and molecular beam deposition (MBD) technique are introduced in chapter II. The experimental procedures for CIGS thin film fabrication, especially by selenization of precursor metallic layers are presented in chapter III. In chapter IV, the results obtained from the characterization techniques are exhibited and discussed. And the study is then summarized in the last chapter.

CHAPTER II
BASICS of CIGS MATERIALS and DEVICES

2.1 Solar cell operation principles

The solar cells are electronic devices that can convert photon energy to electrical energy by photovoltaic (PV) phenomenon that occurs in two types of semiconductor. The connection of p-type and n-type semiconductors forms a p-n junction. When an electron gains energy from, for example, thermal excitation and photon absorption, it undergoes a transition from a valence band to a conduction band leaving a hole (positive charge) in a valence band as shown in Fig 2. The two type carriers are electrons and holes in the semiconductors. The majority carriers in a p-type semiconductor are holes while the majority carriers in an n-type semiconductor are electrons [16].

When the p-type semiconductors are connected with the n-type semiconductors as shown in Fig 3, majority carriers diffuse from the area of higher density to the area of lower density. Electrons diffuse from n-type to p-type while holes diffuse from p-type to n-type until equilibrium is reached. The gradient of potential energy due to the distribution of these carriers at the p-n interface leads to occurrence of built-in electric fields. At the p-n junction, electrons and holes are swept by influence of the electric fields. So the area that deplete of charge carriers is called space-charge region (SCR).

When light is illuminated on a solar cell, materials will absorb a photon if the photon energy is greater than or equal to their band gap energy (E_g). Therefore, a pair of electron and hole is generated. After that, these carriers are separated by built-in electric fields; electron drifts to n-type while hole drifts to p-type. An electron can move from front to back electrodes to recombine with a hole if an external load is connected to solar cells, resulting in the photocurrent collection [16].

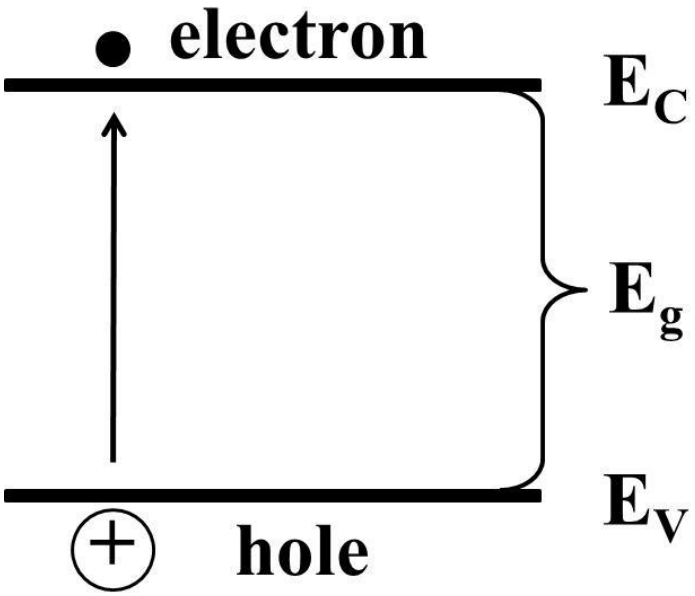

Figure 2 Band diagram of Semiconductor showing electron-hole pair generation.

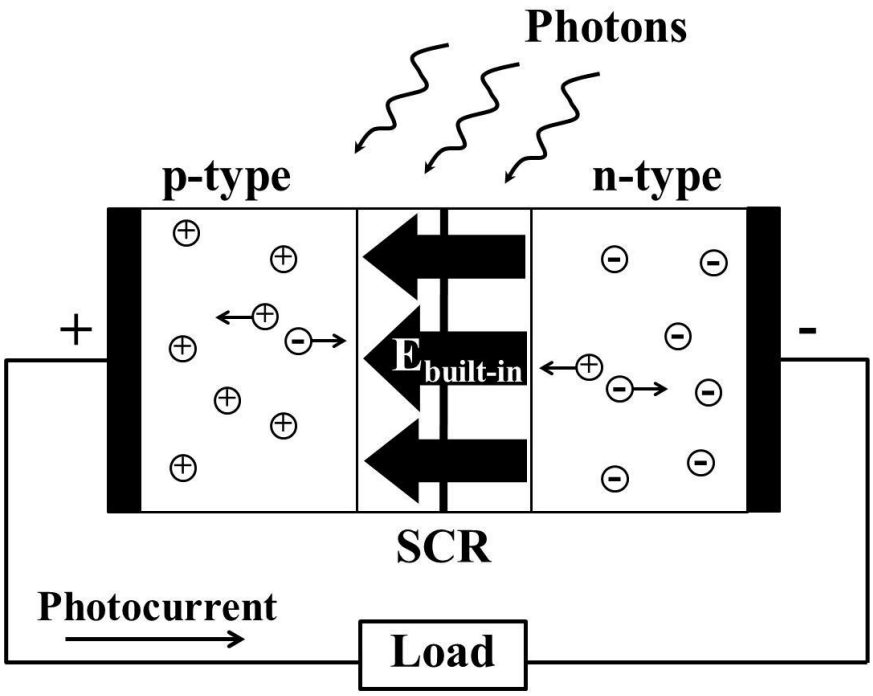

Figure 3 Schematic diagram of a p-n junction solar cells.

2.2 Cu(In,Ga)Se_2 materials

$CuIn_{1-x}Ga_xSe_2$ or CIGS is an alloyed semiconductor in group of I-III-VI_2. The energy band gap (E_g) is the range of 1.04 eV to 1.68 eV by varying the *x* value (between 0 and 1) which is the ratio of Ga to group-III elements (In and Ga atoms) [17].

The crystal structure of CIS, CGS and CIGS belong to the tetragonal chalcopyrite structure which is derived from stacking of two zinc blende crystals. Figure 4 shows the tetrahedral coordination of lattice elements – Se atoms have two bonds to In/Ga and two bonds to Cu atoms. Each of Cu and In/Ga atom has four bonds to Se atoms. In case of CIGS, its tetragonal structure has a-axis and c-axis of 5.7821 Å and 11.6191 Å, respectively [18].

Figure 5 shows ideal solar cell efficiency of CIGS and other materials as a function of bandgap energy under illumination of natural sunlight or AM1.5 condition. Bandgap matching to solar energy of CIGS and its ability to be high efficiency solar cells are advantages of using this material.

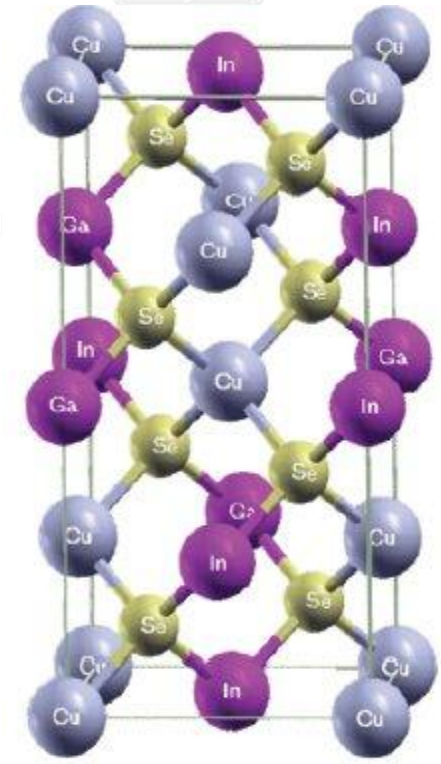

Figure 4 Crystal structure of chalcopyrite CIGS [19].

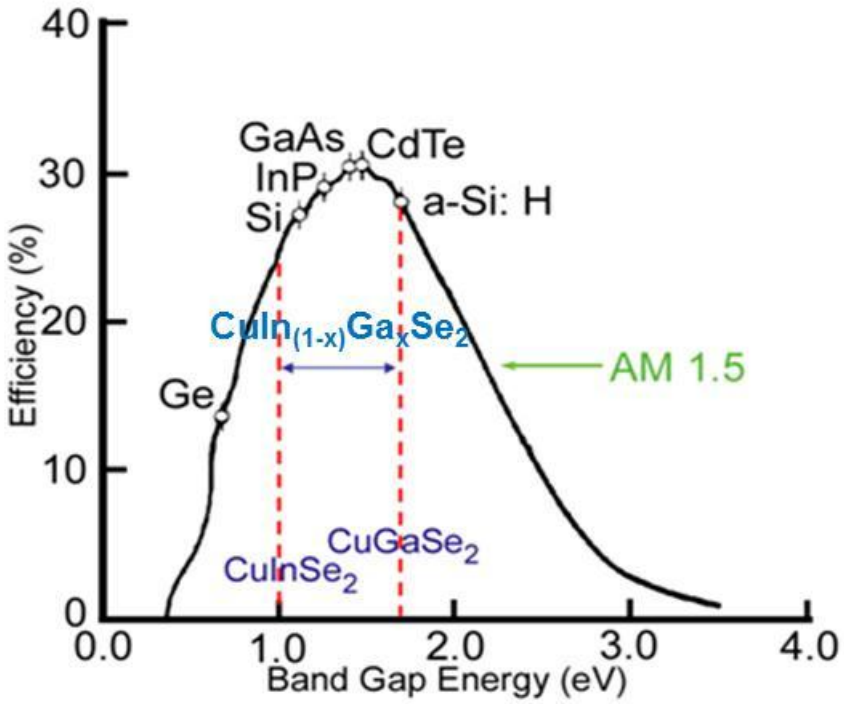

Figure 5 Ideal solar cell efficiency as a function of bandgap energy at AM1.5 [18].

2.3 Molecular beam deposition technique (MBD)

The formation of the CIGS absorber on Mo/SLG substrate can be achieved by molecular beam deposition technique (MBD). The MBD system consists of a main growth chamber and a load lock chamber as seen in Fig. 6. In the growth chamber, it contains Cu, Ga, In and Se sources known as Knudsen cells (K-cells) or effusion cells. It works under the ultrahigh vacuum environment (~10^{-10} Torr) to achieve a large mean free path [17]. The calibration of deposition rates and source temperatures are done using the quartz crystal monitor (QCM) as shown in Fig. 7.

2.4 Calculation of the CIGS deposition rates

The relationship between the deposition rate and the effusion cell temperature is given by

$$\ln(r) = \frac{a}{T} + b\,, \qquad (2.1)$$

where r is the deposition rate (Å/s),

T is the effusion cell temperature (°C),

a and b are parameters form fitting graph with the least-square method.

A method of lease square is employed to obtain the values of parameters *a* and *b* for each source. Thus, the deposition rate of each element must be known, especially Cu deposition rate that depends on the required thickness of CIGS film as shown in Eq. (2.2) and (2.3).

$$r_{Cu} = \frac{d_{Cu}}{t_{Cu}}, \tag{2.2}$$

$$\frac{d_{Cu}}{d_{CIGS}} = \frac{N_{Cu} \cdot \alpha_{Cu}}{N_{CIGS} \cdot \alpha_{CIGS}} = \frac{N_{Cu} \cdot M_{Cu} \cdot [\rho_{CIS}(1-x) + \rho_{CGS}(x)]}{N_{CIGS} \cdot [M_{Cu} + M_{In}(1-x) + M_{Ga}(x+2)M_{Se}]\rho_{Cu}}, \tag{2.3}$$

where r_{Cu} is the deposition rate of Cu (Å/s),

d_{Cu} is the thickness of Cu (Å),

t_{Cu} is the time for deposition of Cu (s),

N_{Cu} is the number of Cu atoms,

N_{CIGS} is the number of CIGS molecules, the N_{Cu} / N_{CIGS} are set to unity,

ρ_i is the density of each element,

and M_i is the molecular mass of each element.

The rate of Ga (r_{Ga}) and In (r_{In}) can be calculated from

$$r_{Ga} = \frac{x}{y} \cdot \frac{\alpha_{Cu}}{\alpha_{Ga}} \cdot r_{Cu} \tag{2.4}$$

and

$$r_{In} = \frac{(1-x)}{y} \cdot \frac{\alpha_{Cu}}{\alpha_{In}} \cdot r_{Cu}, \tag{2.5}$$

where x is the ratio of Ga to group III elements $\left(\frac{[Ga]}{[Ga]+[In]}\right)$ and y is the ratio of Cu to group III elements $\left(\frac{[Cu]}{[Ga]+[In]}\right)$.

The parameter α_i is defined as the ratio of the ρ_i to the M_i of each element that it shown in Table 2.

$$\alpha_{Cu} = \rho_{Cu} \cdot M_{Cu}^{-1}, \tag{2.6}$$

$$\alpha_{In} = \rho_{In} \cdot M_{In}^{-1}, \tag{2.7}$$

and

$$\alpha_{Ga} = \rho_{Ga} \cdot M_{Ga}^{-1}. \tag{2.8}$$

Substitution of r_{Cu}, r_{Ga} and r_{In} into Eq. (2.1) as well as parameters *a* and *b* from obtained from the lease square fitting of the data shown in the graphs of Fig. 7, the working temperature of each element is achieved [5].

The details for the CIGS thin film fabrication in this work are described in the chapter 3.

Table 2 Density, molecular mass and α_i parameter of the material used in CIGS absorber fabrication process.

Material	ρ **(g/cm^3)**	M **(g/mol)**	$\alpha = \rho / M$ **(mol/cm^3)**
Cu	8.96	63.55	0.1410
In	7.31	114.82	0.0637
Ga	5.91	69.72	0.0848
Se	4.79	78.96	0.0607
CIS	5.89	336.29	-
CGS	5.27	291.19	-

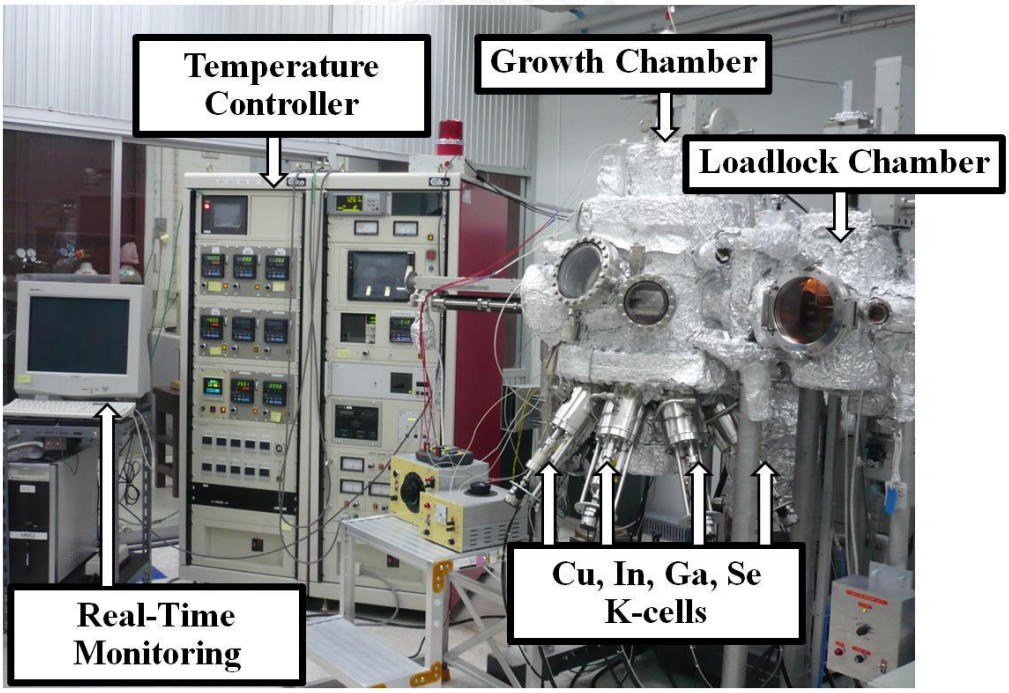

Figure 6 Photograph of Eiko EW100 MBE system.

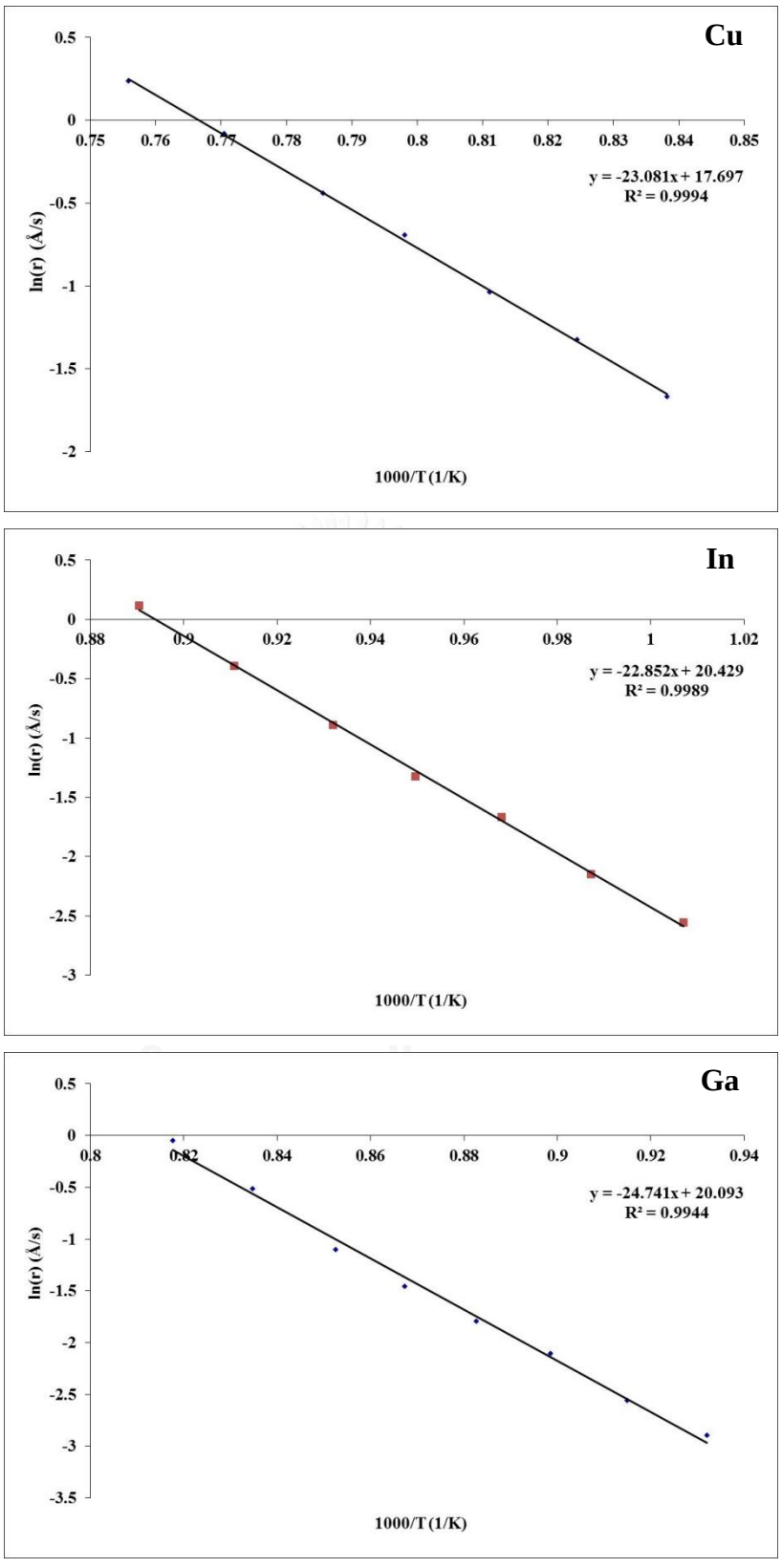

Figure 7 Examples of deposition rates of Cu, In and Ga measured by QCM.

CHAPTER III
EXPERIMENTAL PROCEDURES

In this chapter, I will describe the fabrication of the CIGS solar cells and the application of the growth processes of the CIGS absorber layer. The growth processes are performed by varying sequences of metallic compound layers, substrate temperature and deposition time. The as-grown CIGS absorbers are investigated by FESEM and XRD measurements in order to observe surface morphologies as well as cross–section images and the crystal orientation of CIGS phase. Finally, the solar cell devices are characterized for both I-V characteristic and external quantum efficiency (EQE) measurements in order to study the properties of the devices for the corresponding deposition procedures.

3.1 General fabrication processes for CIGS thin film solar cells

The standard device structure of CIGS solar cells on soda-lime glass (SLG) substrates comprises molybdenum (Mo), p-type CIGS absorber layer, n-type cadmium sulfide (CdS), intrinsic zinc oxide (i-ZnO), aluminum-doped zinc oxide doped (ZnO(Al)) and aluminum (Al) grids as depicted in Fig. 8 [20]. The deposition details are mentioned in the next sub-section, especially the CIGS obtained from the metallic precursors.

3.1.1 Mo back contact

A Mo metal layer is used as a back-contact of the CIGS thin film solar cells for holes transportation. Mo by itself has a melting temperature of 2623ºC which is much higher than the deposition temperature of CIGS films. In addition, Mo layer has a good adhesion property to the SLG substrate due to matching thermal expansion coefficient between the Mo layer and the SLG substrate [21]. In this experiment, the Mo layer is coated on the SLG substrates by sputtering technique from a Mo target (4-inch diameter). The sputtering is done in Argon atmosphere at 6×10^{-3} mbar with the DC sputtering power of 550 Watt for 12 minutes throughout the process. The thickness of the Mo layer is about 0.6 μm.

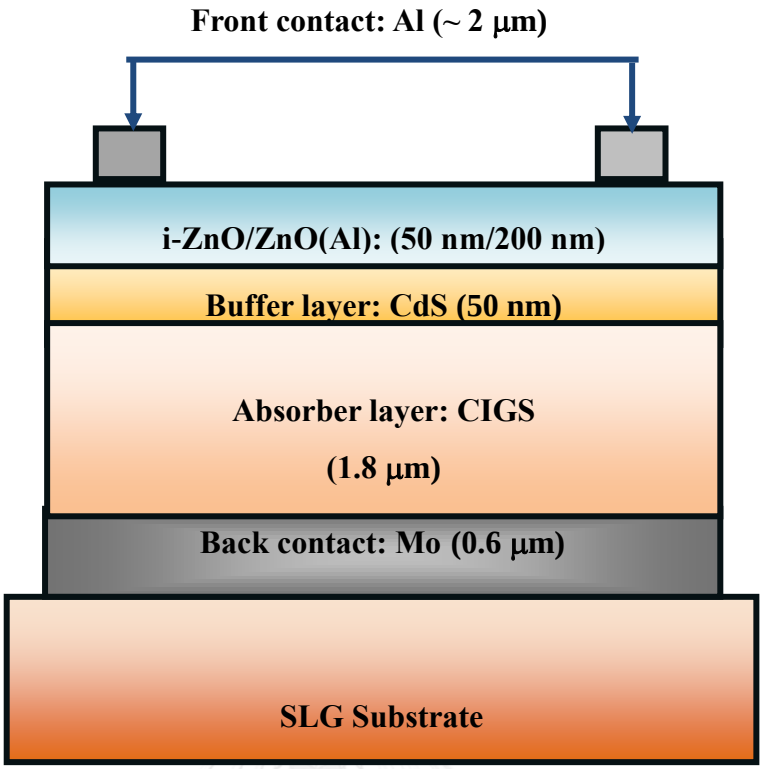

Figure 8 Schematic diagram of the CIGS thin film solar cell structure.

3.1.2 CIGS absorbers fabrication

In this study, the CIGS thin films are fabricated by the multi-sources co-evaporation process (Cu, In, Ga and Se elements). However, the sequences of deposition of the metallic elements are performed to mimic the co-sputtering method for metallic precursors in order to study the CIGS thin films formation

3.1.2.1 Fabrication of CIG metallic precursors

Firstly, the co-evaporation of metallic Cu-In-Ga (CIG) precursors on the Mo/SLG substrates are done at various substrate temperatures, e.g. 120°C, 150°C and 450°C. The precursor thickness is 1.8 μm which is obtained from 1 hour deposition time. The as-grown precursor surfaces are investigated by a field emission scanning electron microscope (FESEM) in order to compare the film morphology at each substrate temperature.

3.1.2.2 Fabrication of CuGa/In and In/CuGa precursors

Common strategies for metallic precursor deposition by the co-sputtering process are typically done by sequences of Cu-Ga/In or In/Cu-Ga [11]. Thus, this experiment is also designed to study the effect of the order of depositions of Cu-Ga and In to investigate the formation of the metallic precursors as schematically shown in Fig. 9. Many studies have found that In, at high substrate temperature, causes the agglomeration of the precursor due to large surface mobility and low melting temperature of In [7]. Then, the substrate temperature for In layer must be as low as 150°C or below. However, it is found in this work that CuGa layer fabricated at low temperature has a serious adhesion problem with the Mo/SLG substrates. In that manner, Cu-Ga metallic layer is deposited on the substrate at high substrate temperature of 450°C. The x value is set for 0.4. FESEM investigation is also used for comparing the surface morphologies in both cases.

(a)

(b)

Figure 9 Schematic diagram of the precursor layers with changing of the order of depositions of Cu-Ga and In; (a) the first layer is In and the second is Cu-Ga, (b) the first layer is Cu-Ga and the second is In.

3.1.2.3 Incorporation of Se into the CIG precursor layers

According to the literatures [5, 22], the homogeneous formation of CIGS thin films should be assisted by copper-selenide (Cu-Se) quasi-liquid phase that can enhance the diffusion of Ga and In at the temperature above 400°C. Then, the incorporation of Se into the precursor layer is achieved by means of Cu-Se co-evaporation at 450°C after the deposition of the precursor layer as shown in Fig. 10. The ratio of Cu to In and Ga from the stages of Cu-Ga and Cu-Se depositions is set for with y = 0.9. The duration of Cu-Se deposition is 30 minutes. The substrate temperature for the deposition of Cu-Ga is set at 450°C and then reduced to 100°C during the deposition of In. Then, the substrate temperature is again increased to 450°C for the Cu-Se deposition, and followed by pure Se vapor for 15 minutes. The cross-section and crystalline structure are investigated by FESEM and XRD, respectively.

The last factor to optimize the homogeneous CIGS thin film growth is the annealing process that is widely used in the fabrication processes. The annealing temperature is 450°C and the annealing times under studies are 1 and 2 hours. The duration of Cu-Se deposition is changed to 40 minutes as shown in Fig. 11. The example of working temperatures for the metallic sources corresponding to the calculation of the CIGS rates described in chapter II is concluded in Table 3. The cross-section images and crystallographic structure of the films are compared. It is noted here that the optimum of homogeneous CIGS film is then chosen for the fabrication of solar cells.

Table 3 Parameters of the growth process.

Parameters	**Required data**
d_{CIGS}	1.8 μm
$t_{Cu,,}$ t_{Ga}, t_{In}	4800 s, 2400 s, 2400 s
X	0.40
Y	0.90
Parameters	**Acquired data**
d_{Cu}	2270.92 Å
r_{Cu}	0.473 Å/s
r_{Ga}	0.694 Å/s
r_{In}	1.394 Å/s
T_{Cu}	978°C
T_{Ga}	936°C
T_{In}	864°C

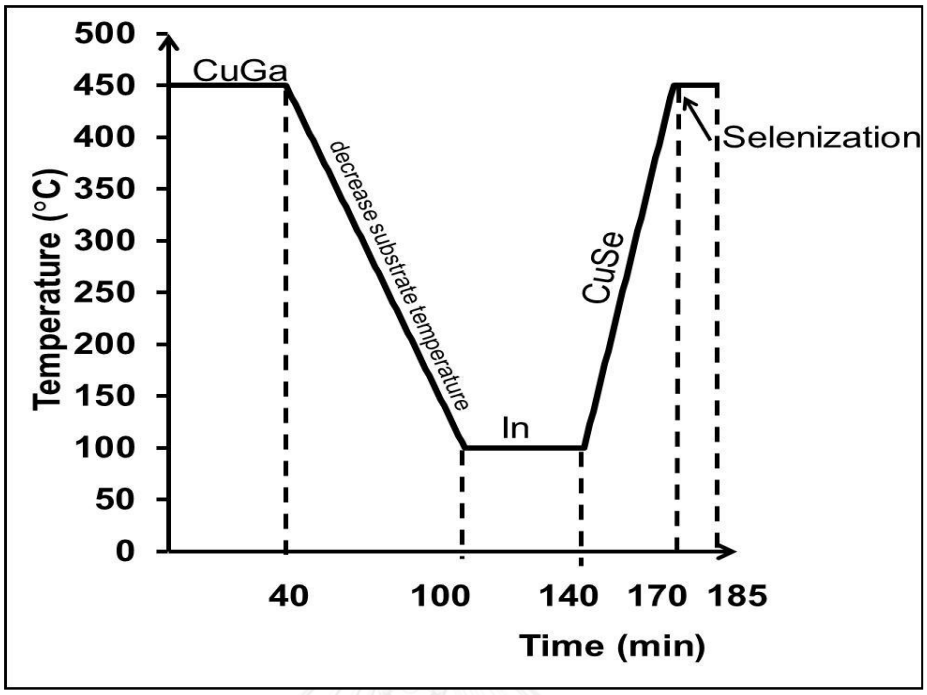

Figure 10 Substrate temperature profile for the fabrication of CIGS absorber from In/Cu-Ga precursor with the addition of Cu-Se and selenization.

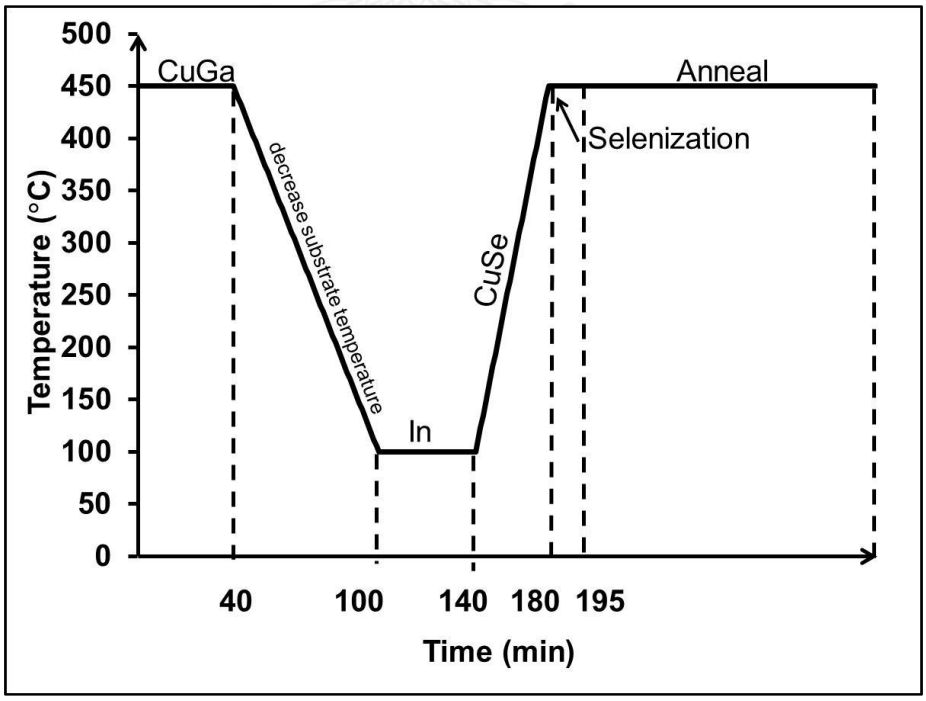

Figure 11 Substrate temperature profile for the fabrication of CIGS absorber from In/Cu-Ga precursor with the addition of Cu-Se, selenization and annealing process.

3.1.3 CdS Buffer layer

A CdS buffer layer is the next thin film layer grown on the CIGS surface by chemical bath deposition (CBD) technique [23]. The bandgap energy of CdS is about 2.4 eV. The beneficial of CdS buffer layer is used to protect the CIGS surface during the growth of ZnO. The thickness of CdS is about 50 nm.

The CdS film is prepared by the mixing of $CdSO_4$ solution (0.3456 g in 50 ml of deionized (DI) water), 25% ammonia solution of 80 ml and $SC(NH_2)_2$ solution (2.85 g in 100 ml of DI water) in 270 ml DI water. The CIGS absorber on Mo/SLG substrate is dipped in the mixed solution at the bath temperature of 65°C for 15 minutes by under the circulation of solution by stirring at 150 rpm.

3.1.4 Window layer

An i-ZnO and a ZnO(Al) are used as a window layer for the CIGS solar cells [24]. i-ZnO is the first layer of high resistive material (50 nm thick and E_g = 3.3 eV) which is used to prevent current leakage. This layer has a good optical transmission. The second layer is ZnO(Al) (200 nm thick and E_g = 3.6-3.8 eV) which has a low resistivity. The i-ZnO and ZnO(Al) layers in this work are deposited by RF magnetron sputtering from a ZnO target and a ZnO(Al) target under Ar presseure of 6×10^{-3} mbar for both layers. The sputtering power and deposition time are set at 40 Watt for 20 minutes and 220 Watt for 17 minutes for the i-ZnO and ZnO(Al), respectively.

3.1.5 Al-grids

In general, the CIGS solar cells use Al-grids as a current collection or a front contact. The Al-grids are thermally evaporated through a metal shadow onto the ZnO(Al) window layer at the base pressure of $\sim 8\times10^{-6}$ mbar. The thickness of the Al-grid layer is about 2 μm [17].

3.2 Characterization techniques

The characterizations of CIGS thin films and devices are performed FESEM, XRD, I-V and QE measurements. The as-grown CIGS films are mainly characterized

by FESEM and XRD. The CIGS thin film solar cells are mainly investigated by I-V and QE measurements.

3.2.1 Field Emission Scanning Electron Microscopy (FESEM)

JEOL JSM 7001 FESEM (as shown in Fig 12) is used to investigate the surface morphology as well as the cross section for the lateral and vertical grain growth of the metallic precursor [25]. It is used to study microstructures or nanostructures of matters. The energy of the electron beams that used for this research is the range of 15-30 kV. The FESEM is also equipped with the energy dispersive X-Ray spectrometer (EDS) to investigate constituent elements of the materials being studied.

Figure 12 The image of JEOL JSM 7001 FESEM.

3.2.2 X-Ray Diffraction (XRD)

This technique is used to determine the crystallographic structure and the shape of the unit cell. The Bruker D8 Advance X-ray powder diffractometer using Cu-target emitted the wavelength of $Cu_{K\alpha 1}$ and $Cu_{K\alpha 2}$ radiations with the wavelengths of 1.5406 Å and 1.54439 Å at 40 kV, respectively [26]. When the beam of X-rays incident on a sample, it is diffracted from the crystal plane obeying the Bragg's law. The path difference is related to the distance of each crystal plane (d) as demonstrated in Fig 13 [27].

$$2d_{hkl}\sin\theta = n\lambda, \tag{3.1}$$

where d_{hkl} is the inter-planar spacing of the crystal plane,

θ is the Bragg's angle,

λ is the wavelength of x-ray ($\lambda_{Cu_{K\alpha 1}} = 1.5406\,\text{Å}$ and $\lambda_{Cu_{K\alpha 2}} = 1.54439\,\text{Å}$),

and n is equal to one for the first order of diffraction.

In this work the appearance of $CuIn_{1-x}Ga_xSe_2$ (CIGS) phase is chalcopyrite with (112) preferred orientation, that angle 2θ appeared in the range of 25° – 30°. Due to the unit cell of the chalcopyrite structure that is tetragonal structure; the lattice constants can be determined from

$$\frac{1}{d^2} = \frac{h^2 + k^2}{a^2} + \frac{l^2}{c^2}, \tag{3.2}$$

where h, k and l are the Miller indices of crystal planes, a and c are the lattice constant parameters.

Scherrer's formula

The relationship of the full width at half maximum (FWHM) and grain size G is described by Scherrer's formula [26] :

$$G = \frac{0.9\lambda}{FWHM\cos\theta}, \qquad (3.3)$$

where λ is the wavelength of $Cu_{K\alpha1}$ (1.54056 Å) and θ is the Bragg's angle in degree from the XRD pattern. Thus, by measuring the FWHM, grain size of the crystal can then be obtained. These grain sizes are inversely related to the FWHM of an individual peak. The narrower of the peak, the larger of the crystallite size.

3.2.3 I-V measurement

When the CIGS solar cell fabrication is complete, it will be investigated by the I-V measurements. The I-V measurement set-up consists of a DC xenon lamp and a voltage source/current measurement unit (Keithley model 237). The device is analyzed under AM1.5 condition at room temperature (25^oC) with the light intensity of 100 mW/cm^2. The information processing is run by Agilent VEE program. The parameters of solar cell consist of open-circuit voltage (V_{OC}), short-circuit current density (J_{SC}), fill factor and efficiency that is determined from the I-V curve.

3.2.4 QE measurement

Quantum efficiency (QE) measurement is used to investigate the photoresponse of CIGS solar cells. By illuminating a device with monochromatic lights form, in case of CIGS solar cells, infrared (1300 nm) to ultraviolet (300 nm), the information of photocurrent collection for each photon wavelength are revealed as a QE curve. Since the photon absorptions and carrier collections in each material thin film layer response to different photon energies, QE results then generally yield the properties of each layer comprising the cells. In this work, only external QE (EQE) is performed on all devices. In general, the integrated areas under EQE curves indicate the whole photogenerated currents that solar cells can produce to external load. The

absorption edges at the long wavelengths imply the beginning of the photon absorption, so correspond to the bandgap energy of the absorber [28, 29].

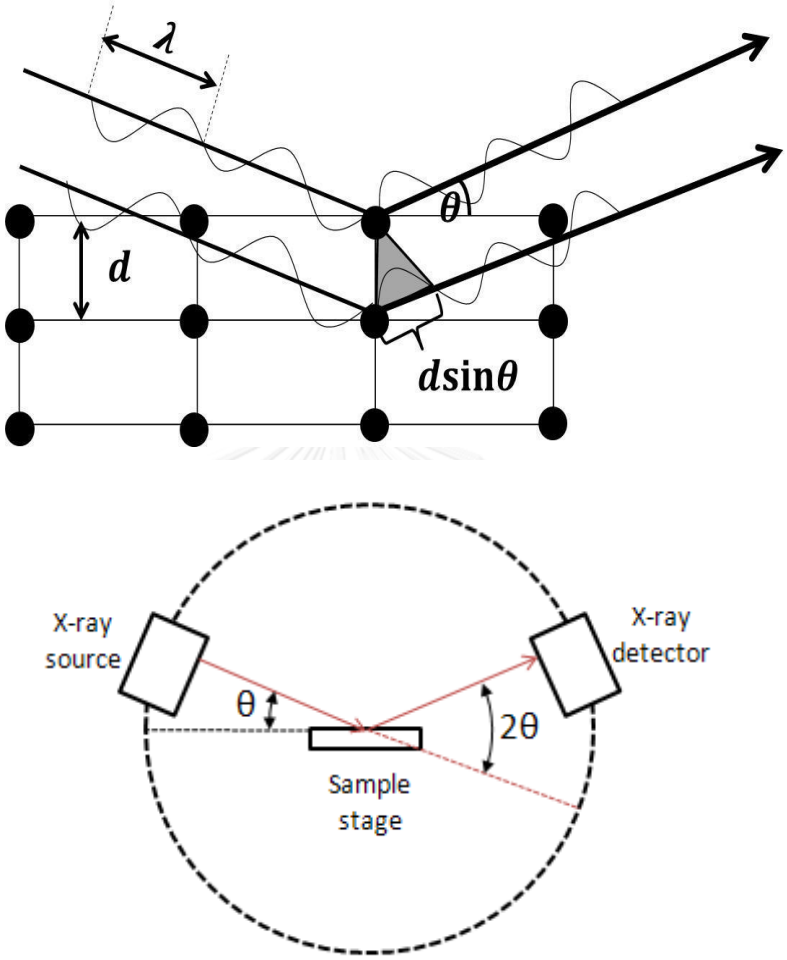

Figure 13 Schematic illustration of the diffractometer for crystal analysis [30].

CHAPTER IV
RESULTS AND DISCUSSION

The experimental results will be shown in this chapter to exhibit the effect of substrate temperature, order of metallic depositions, incorporation of Cu-Se to metallic precursors and annealing process. The influences of different metallic growth sequences on the properties of CIGS absorbers and crystalline structure are presented and discussed. Thereafter, the suitability of more homogeneous CIGS film for solar cell fabrication will be performed in the remainder of the chapter.

4.1 Effect of substrate temperature for the growth of metallic Cu-In-Ga (CIG) precursors

An investigation of the surfaces of CIG metallic thin films at substrate temperature 120°C, 150°C and 450°C is shown in Fig. 14. Both small and large grains of Cu-Ga-In mixture are formed at 120°C and 150°C as shown in Fig. 14 (a) and (b). The EDS measurements show more concentration of In in the area of larger islands. The CIG precursor tends to agglomerate together at 450°C with elongated shapes as shown in Fig. 14 (c). The latter case is due to the low melting point of In that the film pull together at higher substrate temperature. The space between the islands in Fig. 14(c) is the underneath Mo surface. Thus, the simultaneous co-evaporation of Cu, Ga and In is not suitable for the growth of precursor, i.e. In should not be deposited at the same time as Cu and Ga.

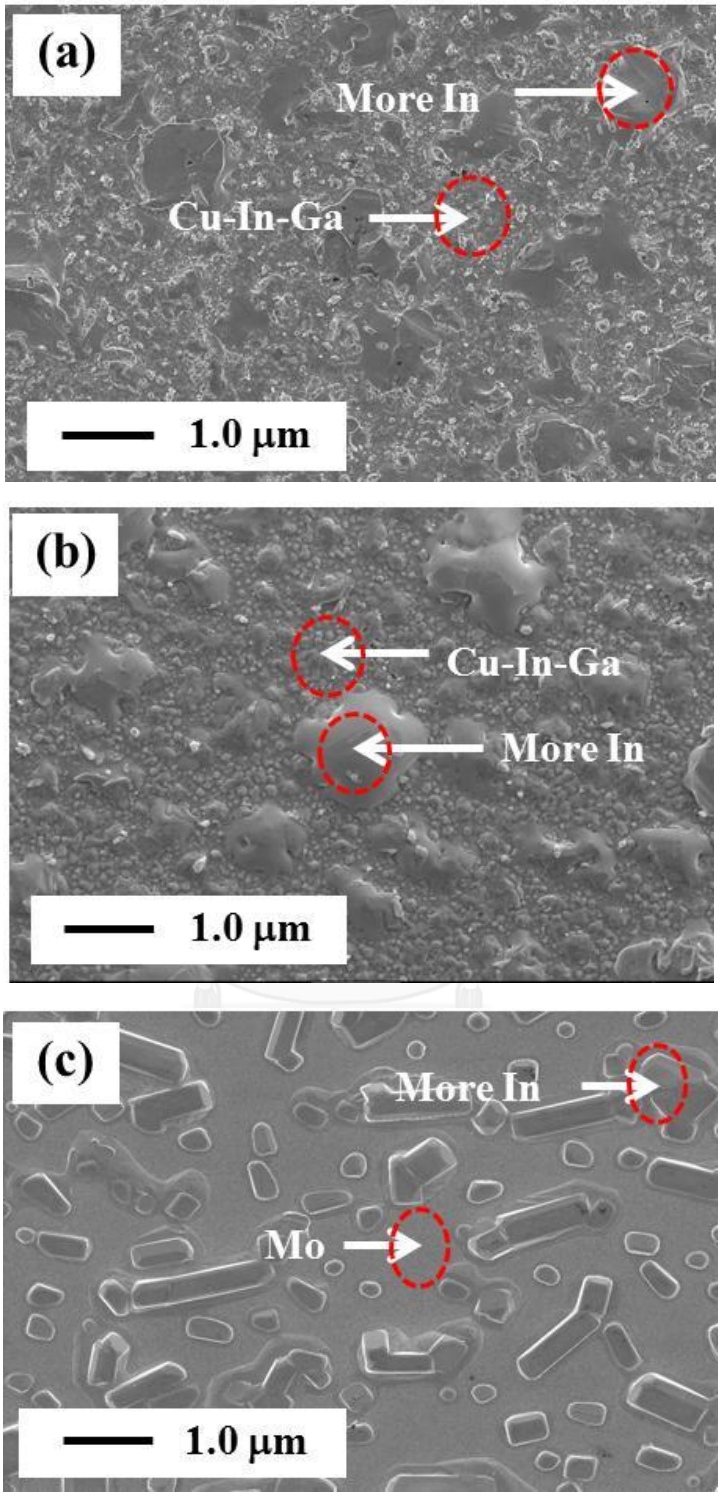

Figure 14 FESEM images of the surfaces of CIG precursors at substrate temperature of (a) 120°C, (b) 150 °C, and (c) 450°C.

4.2 The order of CuGa/In and In/CuGa deposition

In order to avoid agglomeration of the precursors, the sequences of CuGa and In are then considered in this study. The FESEM images in Fig. 15 (a) and (b) show the formation of the metallic precursors of CuGa/In/Mo/SLG and In/CuGa/Mo/SLG, respectively. It can be seen that when In is deposited prior to Cu-Ga, it causes the agglomeration of the precursor, leaving some area exposed to Mo surface as shown in Fig. 15 (a). On the other hand, when Cu-Ga is deposited first and followed by In, more uniform grains of the precursor layer is obtained leaving no area of Mo surface to be observed. It is noted here that some large islands are still visible. This suggests that the Cu-Ga layer must be deposited prior to In. FESEM surface comparison for both samples show that the morphology of Fig. 15 (b) is more uniform than the morphology of Fig. 15 (a). Thus, the deposition of CuGa in the first layer and In layer on the top enhances the uniformity of surface morphology. However, some islands are still seen. As a result, the precursors as shown in Fig. 15 (b) will be further used in the investigation of Se incorporation.

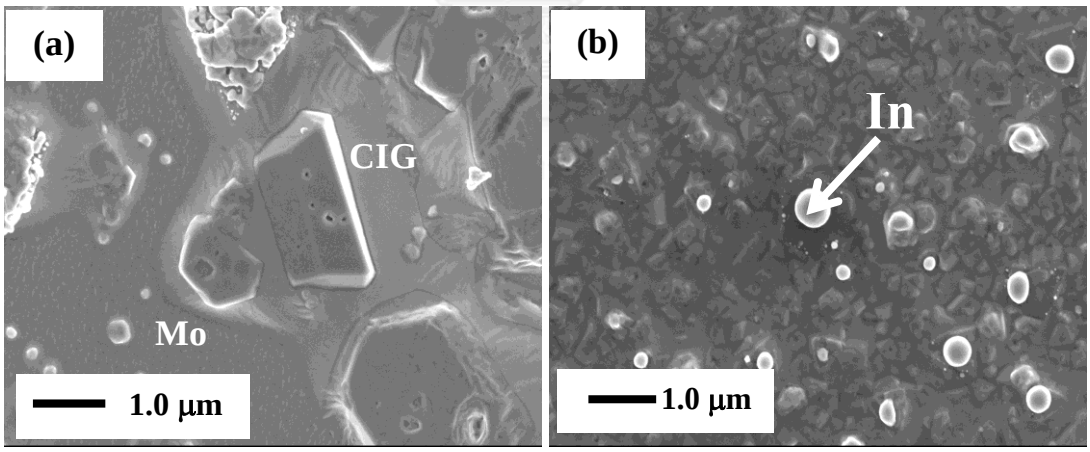

Figure 15 FESEM images of CIG morphologies on Mo-coated SLG substrates; (a) CuGa/In/Mo/SLG, and (b)In/CuGa/Mo/SLG.

4.3 Incorporation of Cu-Se to metallic precursors

When a metallic In/CuGa precursor layer on Mo/SLG substrate is complete, Se is incorporated into the precursor layer by means of Cu-Se co-evaporation at 450ºC. The duration of Cu-Se deposition is 30 minutes. Surface morphology and cross-section images are shown in Fig. 16. The surface of the film shows random orientations of elongated shapes with some voids. The cross-section image shows vertical grain growth with some smaller grains at the bottom. The XRD result yields relatively low intensity of chalcopyrite CIGS (112) and (220)/(204) phases. It can also be seen that (112) phase is not pure due to the broadening of the peak. In addition, the film is easy to flake off. To enhance the quality and adhesion of the film to the Mo surface, the deposition time of Cu-Se is increased to 40 minutes. The cross-section images and the XRD patterns are shown in Fig. 17 (a). Larger grains are formed on the top layer with small grains underneath. The XRD shows the (112) preferred orientation of chalcopyrite phase. However, the separated (112) peaks corresponding to CIS and some residue of CIGS at the bottom layer of the film are observed in the XRD pattern of Fig. 17 (a). The comparisons of grain size for the incorporation of Cu-Se for 30 and 40 minutes are shown in Table 4. The grain size of the CIGS film with Cu-Se process time of 40 minutes is considerably larger the 30 minutes one.

Table 4 The calculation of grain size using Scherrer's formula using the peak of CIGS (112) phase.

The deposition time of Cu-Se	**FWHM (degrees)**	**2θ (degrees)**	**θ (degrees)**	**grain size (nm)**
30 min	0.54	26.78	13.39	30
40 min	0.14	26.64	13.32	164

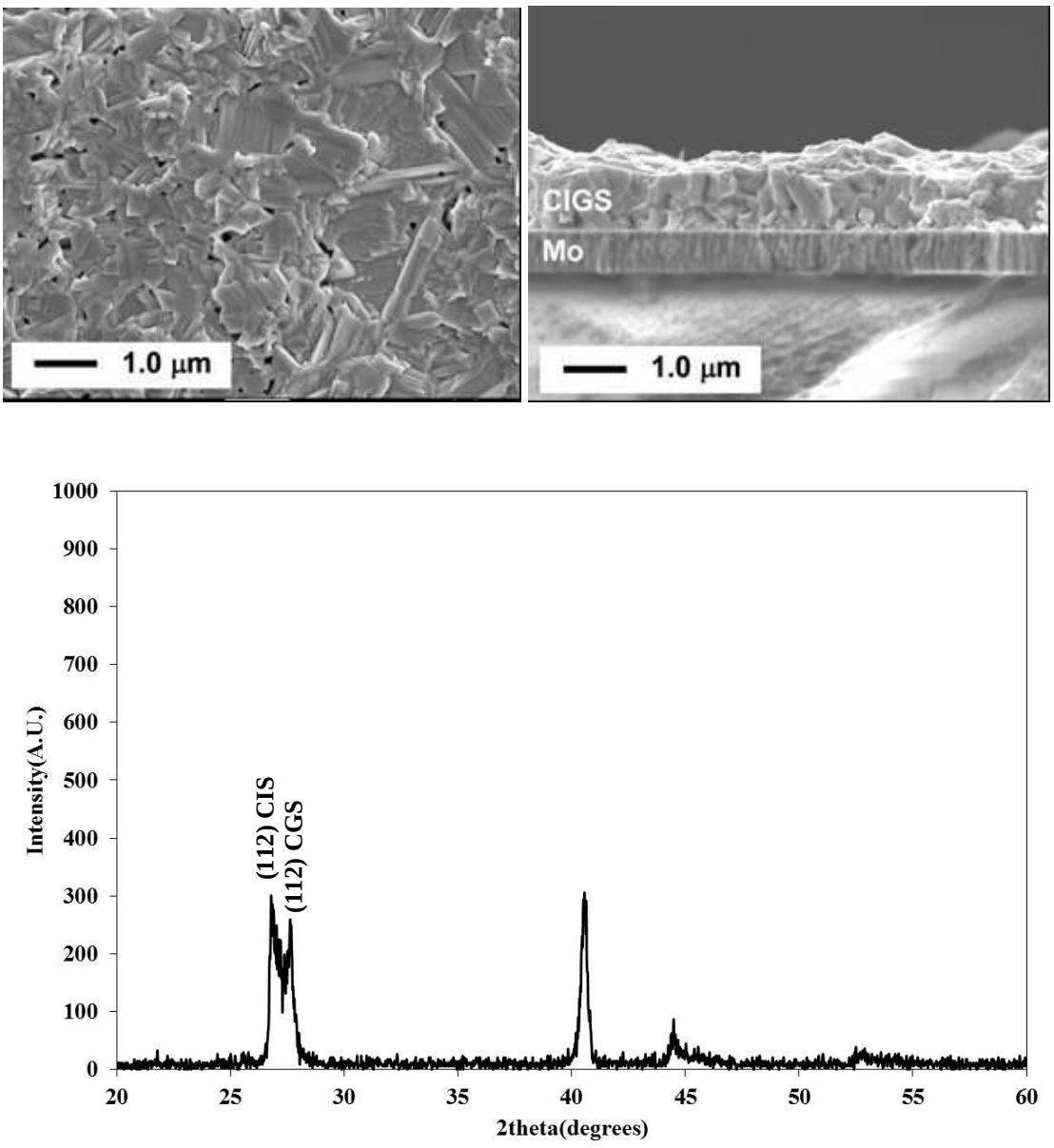

Figure 16 FESEM image (above) and XRD pattern (below) of a sample; selenization/CuSe/In/CuGa/Mo/SLG.

4.4 Annealing process

The residual CIS can be eliminated by vacuum annealing the film after the growth process. The results of annealing for 1 and 2 hours are shown in Fig. 17 (b)-(c), respectively. It can be seen in Fig. 17 (b) that smaller grains are still visible near the bottom of the film and the residue of (112) CIGS phase (with lower intensity) is still seen in the XRD pattern. When the annealing time is increased to 2 hours, larger vertical grain growth is observed as shown in Fig. 17 (c) with no (112) CIS in the XRD pattern. In addition, the grain size of film annealing for 1 and 2 hours are estimated and shown in Table 5. The calculation of grain size for 2 hour annealing is smaller due to more incorporation of Ga in the CIGS film. Then, the CIS is not observed in this case as shown in Fig. 17 (c).

Table 5 The calculation of grain size using Scherrer's formula for the (112) phase of CIGS thin film annealed for 1 hour and 2 hours.

Annealing time	**(112) Intensity**	**FWHM (degrees)**	**2θ (degrees)**	**θ (degrees)**	**grain size (nm)**
1 hour	CIGS	0.08	26.62	13.31	40
	CIS	0.30	27.34	13.67	199
2 hours	CIGS	0.20	26.86	13.43	794

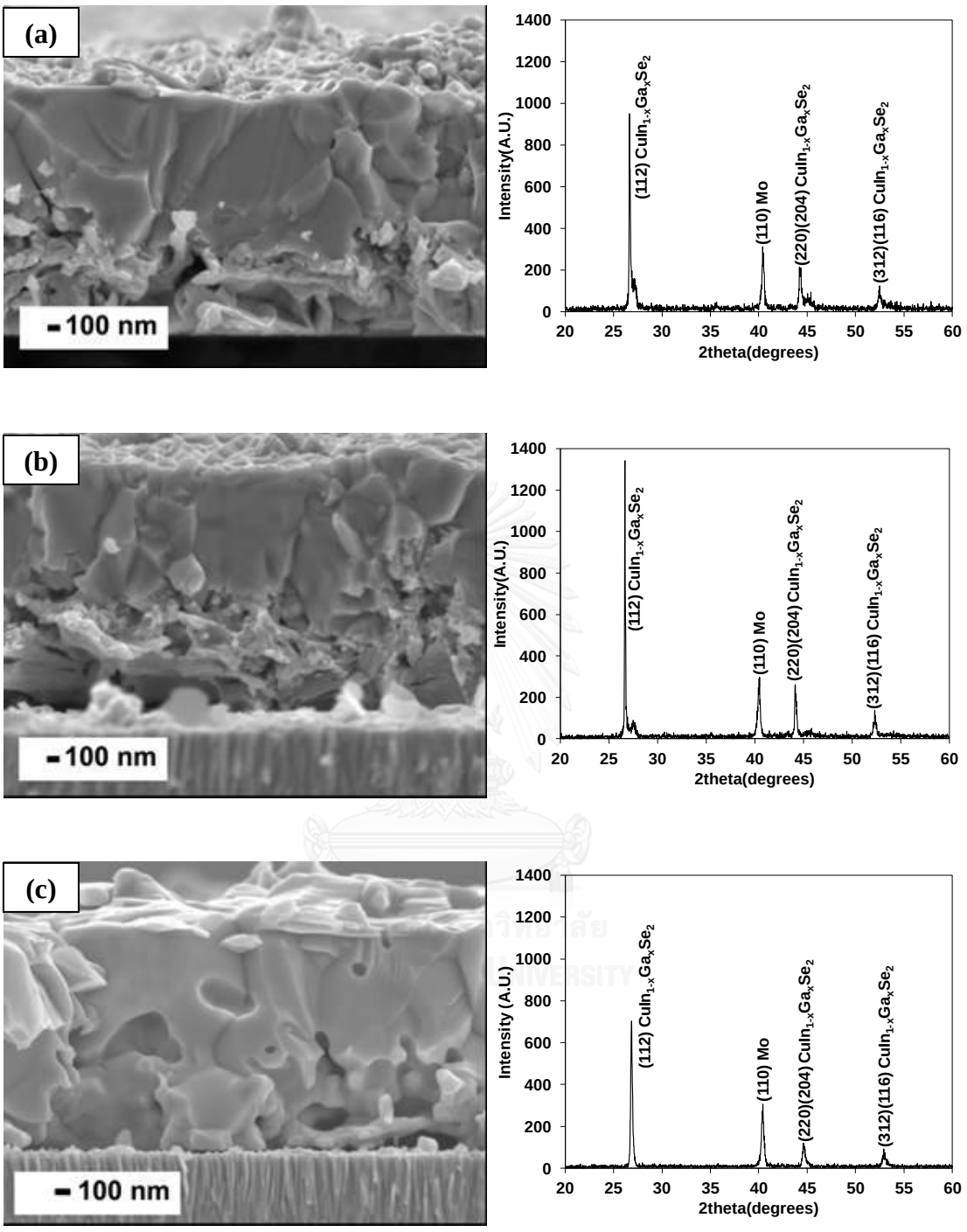

Figure 17 FESEM images (left) and XRD patterns (right) of
(a) CIGS thin film without annealing,
(b) CIGS thin film annealed for 1 hour and
(c) CIGS thin film annealed for 2 hours.

4.5. Performance of the CIGS thin film solar cells

The CIGS absorber with pure (112) phase, shown in Fig. 17(c), is chosen for the fabrication of the solar cells. The average efficiency is about 12.5% with the maximum at 13.2% as shown in Fig. 18. The open-circuit voltage (V_{OC}) and the short-circuit current density (J_{SC}) of the best device is 512 mV and 36.43 mA/cm^2, respectively. The junction formation is quite good, given by the fill factor (FF) of 70.7%.

The spectral response of the devices characterized by the external quantum efficiency measurement is shown in the inset. The threshold for the photon absorption of the device in the long wavelength region begins at about 12000 Å, corresponding to the energy gap of $CuInSe_2$ (1.03 eV). The decrease in the EQE curve at about 5500 Å (2.25 eV) is due to the absorption of photons by the CdS. The EQE is terminated the shortest wavelength of about 3400 Å (3.65 eV) corresponding to the energy gap of ZnO(Al). The integrated area under the EQE curve indicates the whole collected currents that solar cells can produce to external load. The result of EQE indicates that the surface of the absorber layer is CIS rather than CIGS with x = 0.4 as set by the deposition parameters. This implies that there is some nonhomogeneous distribution of group-III elements for the absorber fabricated by this technique that induces the grading in the band gap energy.

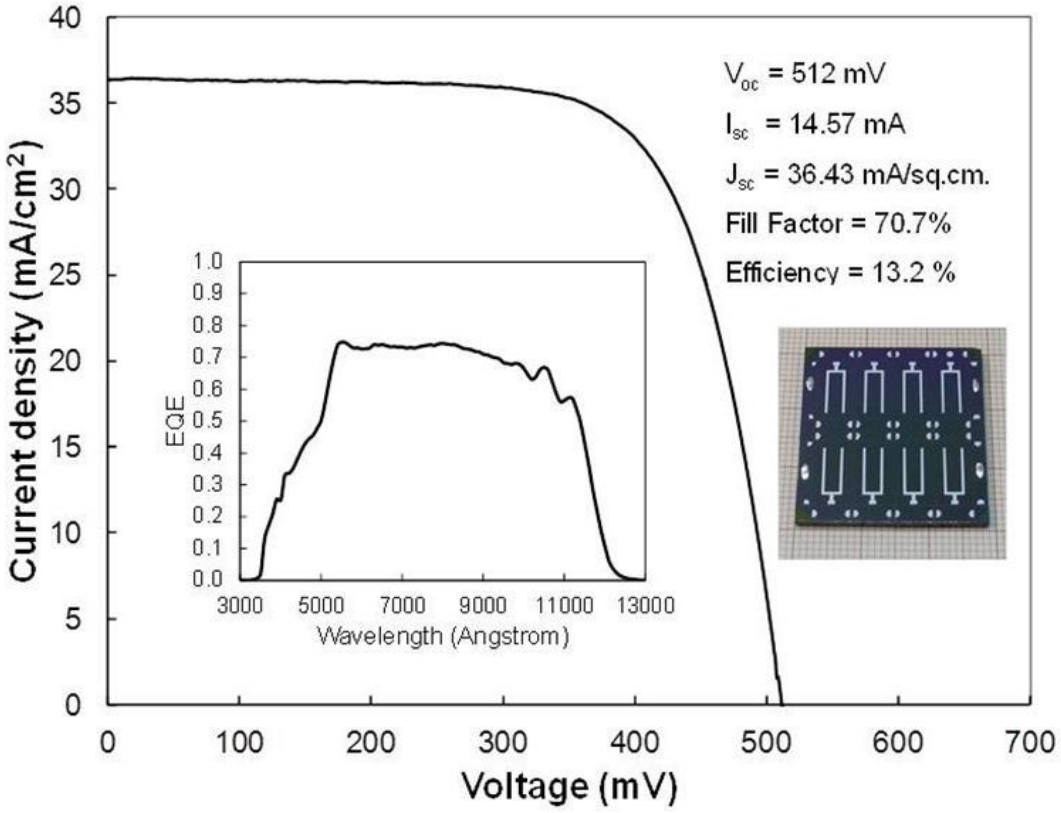

Figure 18 J-V characteristic of the best CIGS thin film solar cell of the film fabricated similar to that of Fig. 17(c). The inset shows the corresponding external quantum efficiency of the device. The picture shows 8 small cells on the 3cm x 3cm substrate, each has an area of 0.5 cm^2.

CHAPTER V
CONCLUSTION

In this study, CIGS thin film solar cells on Mo/SLG substrates were successfully fabricated by co-evaporation and selenization process to mimic the co-sputtering method. To study physical properties and investigate the device performance, substrate temperature, order of metallic depositions, incorporation of Cu-Se to the metallic precursors and annealing time during the fabrication CIGS thin have been investigated. The effects from these factors can be summarized as;

- Effect of co-evaporation of Cu, In and Ga at various substrate temperatures;

The deposition of Cu-Ga-In precursor was done using co-evaporation of Cu, Ga and In fluxes by varying the substrate temperature at 120°C, 150°C and 450°C on the 3cm x 3cm Mo/SLG substrates. At the substrate temperature of 450°C, the precursors tend to agglomerate together with elongated shapes. Nevertheless, substrate temperatures as low as 150°C or below prevent the agglomeration of In. Due to low melting point of In and adhesion issues of the metallic precursors, the substrate temperature was optimized for the depositions of In and Cu-Ga layers. Thus, the co-evaporation of Cu, Ga and In is not suitable for the precursor, i.e. In should not be deposited at the same time of Cu and Ga.

- Effect of sequential depositions of CuGa/In and In/CuGa on Mo/SLG;

The results suggest that the Cu-Ga layer must be deposited prior to In to obtain good adhesion of the film to the substrate. The suitable substrate temperature for the Cu-Ga layer and In layer was 450°C and 100°C, respectively. The higher substrate temperature for the Cu-Ga would enhance the adhesion of the film to Mo surface. The x value was also set for 0.4 in both CuGa/In and In/CuGa depositions.

- Effect of Se incorporation into the precursor layer;

In/CuGa/Mo/SLG was incorporated with Se by means of Cu-Se co-evaporation at 450°C for 30 min, then followed by Se vapor at 450°C for 15 min. The result of XRD pattern shows the doublet of (112) peaks corresponding to CIS and CGS that it is not pure CIGS.

- Effect of the annealing time

The pure (112) CIGS phase was obtained in the film annealed at 450°C for 2 hours. The CIGS solar cell fabrication was completed by the standard procedures and compared with other fabrication methods as summarized in Table 6. The best cell efficiency of 13.2% was obtained and the EQE indicated that the surface of the absorber should be CIS rather than CIGS.

Table 6 Comparison of fabrication methods for CIGS thin films between this work and other methods.

Methods	Advantages	Disadvantages	Efficiencies	Compared with this work
Co-evaporation [4, 6]; evaporate Cu, In, Ga and Se atoms simultaneously	• suitable for studying physical properties • good uniformity	• limit only to lab scale • difficult for large area	21.70%	• use more Se flux
Co-sputtering [7]; fabricate by simultaneous sputtering of two targets (In target and Cu-Ga alloy target)	• high deposition speed • large area films	• difficult control of composition • expensive targets	15.00%	• difficult to adjust the composition of x and y value
Spray solution [8]; aqueous solution containing $CuCl_2$, $InCl_3$, $Ga(NO_3)_3H_2O$ and selenourea was used for precursor solution and vaporized as aerosol before deposition at T_{sub} = 400ºC	• low-cost • use in large-scale production • does not require the use of vacuum	• difficult to control parameters, e.g. solution flow rate, direction growth and non-uniformity	5.00%	• more impurities
Selenization [9]; Se over-vapor after metallic deposition process (T_{sub} = 550 – 650ºC in vacuum system)	• rapid process	• easy agglomerate of In-Se compound	3.48%	• impure (112) CIGS phase
This work co-evaporation imtitating co-sputtering	• pure (112) CIGS phase • good uniformity	• take relatively long time	13.20%	

REFERENCES

1. Fraas, L.M. and L.D. Partain, *Solar Cells and Their Applications*. 2 ed, ed. K. Chang. 2010, Hoboken, NJ, USA: John Wiley & Sons, Inc.
2. U.S. Department of Energy, *The History of Solar*, U.S. Department of Energy, Editor., The Office of Energy Efficiency and Renewable Energy (EERE).
3. *A Short History of Photo voltaic (PV) Cells*. 2006: Genesis Energy.
4. Zentrum für Sonnenenergie- und Wasserstoff-Forschung (ZSW) Baden-Württemberg, *New best mark in thin-film solar performance with 21.7 percent efficiency*. 2014: German state of Baden-Württemberg, together with universities.
5. Namnuan, B., *DIFFUSION OF GALLIUM IN $CuInSe_2$/$CuGaSe_2$ BILAYER THIN FILMS*. 2011, Chulalongkorn University: Chulalongkorn University.
6. Kaelin, M., D. Rudmann, and A.N. Tiwari, *Low cost processing of CIGS thin film solar cells.* Solar Energy, 2004. **77**(6): p. 749-756.
7. Han, J.-f., et al., *An optimized In–CuGa metallic precursors for chalcopyrite thin films.* Thin Solid Films, 2013. **545**(0): p. 251-256.
8. Lee, D.-Y., S. Park, and J. Kim, *Structural analysis of CIGS film prepared by chemical spray deposition.* Current Applied Physics, 2011. **11**(1, Supplement): p. S88-S92.
9. Song, H.K., et al., *Fabrication of $CuIn_{1-x}Ga_xSe_2$ thin film solar cells by sputtering and selenization process.* Thin Solid Films, 2003. **435**(1–2): p. 186-192.
10. The National Center for Photovoltaics (NCPV). *Best Research-Cell Efficiencies* 2015; Available from: http://www.nrel.gov/ncpv/images/efficiency_chart.jpg.
11. Liang, H., et al., *CIGS formation by high temperature selenization of metal precursors in H_2Se atmosphere.* Solid-State Electronics, 2012. **76**(0): p. 95-100.
12. Su, C.-Y., et al., *The effects of the morphology on the CIGS thin films prepared by CuInGa single precursor.* Solar Energy Materials and Solar Cells, 2011. **95**(1): p. 261-263.

13. Harvey, T.B., et al., *Copper Indium Gallium Selenide (CIGS) Photovoltaic Devices Made Using Multistep Selenization of Nanocrystal Films.* ACS Applied Materials & Interfaces, 2013. **5**(18): p. 9134-9140.
14. Hunger, R., et al., *In situ deposition rate monitoring during the three-stage-growth process of Cu(In,Ga)Se_2 absorber films.* Thin Solid Films, 2003. **431–432**(0): p. 16-21.
15. Arthibenyakul, B. and C.a.C. Chityuttakarn, S.,, *The Presence of $CuGaSe_2$ Interface Layer in the Growth of Cu-rich $CuInSe_2$/GaAs(001) Epitaxial Films.* J.Cryst.Growth, 2011: p. 97-100.
16. Hersch, P. and K. Zweibel, *Basic Photovoltaic Principles and Methods*. 1982, United States of America: Solar Energy Research Institute.
17. Sakdanuphab, R., *INFLUENCE OF SODIUM IN FABRICATION PROCESS OF HIGH EFFICIENCY Cu(In,Ga)Se_2 THIN FILM SOLAR CELL*, in *Department of Physics*. 2010, Chulalongkorn University: Chulalongkorn University.
18. THONGKHAM, W., *FABRICATION OF Cu(In,Ga)Se_2 THIN FILM SOLAR CELLS ON FLEXIBLE METALLIC FOILS*, in *Department of Physics*. 2011, Chulalongkorn University: Chulalongkorn University.
19. Gerngroß, M.-D. and Reverey J., *CIS/CIGS BASED THIN-FILM SOLAR CELLS*. Faculty of Engineering University of Kiel.
20. Dhere, N.G., *Present status and future prospects of CIGSS thin film solar cells.* Solar Energy Materials and Solar Cells, 2006. **90**(15): p. 2181-2190.
21. Lepetit, T., et al., *Impact of DC-power during Mo back contact sputtering on the alkali distribution in Cu(In,Ga)Se_2-based thin film solar cells.* Thin Solid Films, 2015. **582**(0): p. 304-307.
22. Arthibenyakul, B., *GROWTH AND CHARATERIZATION OF HIGH QUALITY $CuInSe_2$ EPITAXIAL THIN FILMS ON GaAs SUBSTRATES*, in *Department of Physics*. 2010, Chulalongkorn University: Chulalongkorn University.
23. Abou-Ras, D., et al., *Structural and chemical investigations of CBD- and PVD-CdS buffer layers and interfaces in Cu(In,Ga)Se_2-based thin film solar cells.* Thin Solid Films, 2005. **480–481**(0): p. 118-123.

24. Ma, A., et al., *Study of a low power plasma reactor for the synthesis of zinc oxide as window layers in Cu(In,Ga)Se_2 solar cells.* Thin Solid Films, 2015. **582**(0): p. 345-350.
25. Ogura, T., *Nanoscale analysis of unstained biological specimens in water without radiation damage using high-resolution frequency transmission electric-field system based on FE-SEM.* Biochemical and Biophysical Research Communications, 2015. **459**(3): p. 521-528.
26. Goldstein, J., D.E. Newbury, and Williams D.B., *X-Ray Spectrometry in Electron Beam Instruments*. Vol. 1st. 1995, New York: New York.
27. E Dann, S., *Reactions and Characterization of Solids*. 2000, Loughborough University.
28. Nagle, T.J., *Quantum Efficiency as a Device-physics Interpretation Tool for Thin-film Solar Cells,* in *department of Physics*. 2007, Colorado State University.
29. Castaner, L. and S. Silvestre, *Modelling Photovoltaic Systems Using PSpice*. 1 ed. 2002.
30. Panda, B., *STRUCTURAL AND ELECTRONIC PROPERTIES OF CHALCOPYRITE SEMICONDUCTORS,* in *Department Of Physics*. 2011: National Institute Of Technology, Rourkela.

APPENDICES

APPENDIX A

LIST OF SYMBOLS AND ABBREVIATIONS

Symbols

a	Lattice parameter
a.u.	Arbitrary unit
A	Unit area of the growing film
c	Lattice parameter
d_{CIGS}	Thickness of CIGS
d_{Cu}	Thickness of the Cu element
d_{Ga}	Thickness of the Ga element
d_{hkl}	Inter planar spacing of the crystal plane
E_g	Energy band gap
eV	Energy unit: electron volt
FF	Fill factor
G	Grain size
h	Miller indices
$\mathrm{In_{Cu}}$	Indium substitution to Copper site
I_0	Leak current
$I_{\max}$	Maximum current
I_{sc}	Short-circuit current
J_{sc}	Short-circuit current density
k	Miller indices
k_B	Boltzmann constant
l	Miller indices
M_i	Molecular mass of each element
n	Equal one that it is the first order of diffraction
N_A	Avocadro's constant: 6.02×10^{23} atoms or molecules
N_{CIGS}	Number of CIGS molecules

N_{Cu}	Number of Cu atoms
q	Electron charge
r	Deposition rate
r_{Ga}	Calculation of deposition rate value of Ga
t_{Ga}	Whole time for deposition of Ga element
T	Temperature
Torr	Presure unit
T_m	Melting point temperature
T_{sub}	Substrate temperature
V	Voltage
V_{Cu}	Copper vacancy
V_{max}	Maximum open-circuit voltage
V_{oc}	Open-circuit voltage
y	Copper atomic composition ([Cu]/([Ga]+[In]))
y > 1	Cu-rich composition
y < 1	Cu-poor composition
y = 1	Stoichiometric composition
W	Power unit: Watt
Å	Angstrom (10^{-10}m)
°C	Temperature unit: degree Celsiuus
μm	Micron (10^{-6}m)
η	Conversion efficiency of solar cells
θ	Bragg's angle
ρ_{Cu}	Density of the Cu element
ρ_{Ga}	Density of the Ga element
ρ_i	Density of each element
λ	Wavelength of x-ray
$\lambda_{Cu_{K\alpha 1}}$	Wavelength of x-ray: 1.5406 Å

Abbreviations

Al	Aluminum
AM	Air Mass
Ar	Argon element
bcc	Body centered tetragonal
CBD	Chemical Bath Deposition
CdS	Casmium Sufilde
CdSO4	Cadmium sulfate
CGS	Copper Gallium Diselenide: $CuGaSe_2$
CIGS	Copper Indium Gallium Diselenide: $Cu(In_{1-x}Ga_x)Se_2$
CIS	Copper Indium Diselenide: $CuInSe_2$
Cu	Copper element
$CuCl_2$	Copper (II) Chloride
DI	De-ionized
EDS	Energy Dispersive X-ray Spectroscopy
EQE	External Quantum efficiency measurement
FESEM	Field Emission Scanning Electron Microscopy
fcc	Face centered cubic
FWHM	Full Width at Half Maximun
Ga	Gallium element
$Ga(NO_3)_3$	Gallium hydroxide
H_2O	Water
IQE	Internal quantum efficiency
In	In element
$InCl_3$	Indium(III) Chloride Tetrahydrate
K-cells	Knudsen cells
LDF	Lorentzian Distribution Function
MBD	Molecular Beam Deposition
Mo	Molybdenum
NREL	Nation Renewable Energy Laboratory
PV	Photovoltaic
QCM	Quartz crystal monitor

QE	Quantum efficiency
RF	Radio frequency
$SC(NH_2)_2$	Thiourea
Se	Selenium element
SLG	Soda-lime glass
SPRL	Semiconductor physics research laboratory
XRD	X-Ray Diffraction
ZnO	Zinc oxide

APPENDIX B

LIST OF CONFERENCES

Conference Presentation:

2014 40th Annual Conference of Thai Physics Society (Science and Technology of Thailand STT), December 2-4, 2014, Khon Kaen, Thailand.

VITA

Kwanruthai Butsriruk was born on 11th May 1989 in Roi-Et province, Thailand. She received her Bachelor of Science degree in Physics from Chulalongkorn University, Thailand in 2012.